Lithos 140–141 (2012) 38–52

Contents lists available at SciVerse ScienceDirect

Lithos

journal homepage: www.elsevier.com/locate/lithos

U–Pb zircon age, geochemical and Sr–Nd isotopic data as constraints on the petrogenesis and emplacement time of the Precambrian mafic dyke swarms in the North China Craton (NCC)

Shen Liu [a,b,*], Ruizhong Hu [a], Shan Gao [b], Caixia Feng [a], Ian M. Coulson [c], Guangying Feng [a], Youqiang Qi [a], Yuhong Yang [a], Chaogui Yang [a], Liang Tang [a]

[a] State Key Laboratory of Ore Deposit Geochemistry, Institute of Geochemistry, Chinese Academy of Sciences, Guiyang 550002, China
[b] State Key Laboratory of Geological Processes and Mineral Resources, China University of Geosciences, Wuhan 430074, China
[c] Solid Earth Studies Laboratory, Department of Geology, University of Regina, Regina, Saskatchewan, Canada S4S 0A2.

ARTICLE INFO

Article history:
Received 19 September 2011
Accepted 2 January 2012
Available online 13 January 2012

Keywords:
Mafic dykes
U–Pb ages
Petrogenesis
Precambrian
NCC

ABSTRACT

Precambrian mafic dykes in the North China Craton (**NCC**) consist of dolerite. Geochronological, geochemical, and whole-rock Sr–Nd isotopic analyses were performed on this suite of mafic dykes to characterise their ages and petrogenesis. Laser Ablation-Inductively Coupled Plasma-Mass Spectrometry (LA-ICP-MS) U–Pb zircon analyses yield consistent ages ranging from 837.9 ± 4.8 Ma to 2510 ± 18 Ma for seven of the mafic dykes (SHS01, TDG01, LJZ01, LQS02, HB02, WJ01, and DST01) from NCC. Based on these, the mafic dykes can be divided into three groupings: ~2.4–2.5 Ga, ~1.8–1.9 Ga and 0.8–1.0 Ga. The studied dykes belong to the alkaline and sub-alkaline magma series in terms of $K_2O + Na_2O$ contents (2.6–6.2 wt.%), and to the Tholeiitic, calc-alkaline and high-K calc-alkaline series based on their K_2O contents (0.1–2.1 wt.%). The mafic dykes are further characterised by low and variable light rare earth elements (~2.4–2.5 Ga mafic dykes, $(La/Yb)_N = 3.83–10.4$; ~1.8–1.9 Ga mafic dykes, $(La/Yb)_N = 1.45–2.35$); 0.8–1.0 Ga mafic dykes, $(La/Yb)_N = 0.66–4.27$, show variable Eu anomalies ($\delta Eu = 0.94–1.35$, 0.77–1.21; 0.92–1.28, respectively), positive anomalies in Ba, U, La and Pb, and are depleted in Rb and high field strength elements (Nb, Ta, Ti, and minor Zr and Hf). In addition, the studied mafic dykes all display relatively low radiogenic Sr [$(^{87}Sr/^{86}Sr)_i = 0.6747–0.6921$; 0.7017–0.7025; 0.7005–0.7049, respectively for the ~2.4–2.5 Ga, ~1.8–1.9 Ga and 0.8–1.0 Ga mafic dyke groups] and large $\varepsilon_{Nd}(t)$ (13.2–13.5; 10.4–11.8; 6.5–8.5, respectively). These results suggest that all the mafic rocks were derived from a depleted mantle source hybridised by foundered lower crust. The parent mafic magmas likely experienced fractional crystallisation of olivine, pyroxene, hornblende, plagioclase and Fe–Ti oxides (e.g., rutile, ilmenite, titanite, etc.) during dyke ascent, with negligible evidence for crustal contamination prior to emplacement at a high crustal level.

1. Introduction

Mafic dyke swarms are widespread within the continental lithosphere and are generally formed during lithospheric-scale extension (Féraud et al., 1987; Gudmunsson, 1995; Halls, 1987). The swarms prove particularly useful indicators in the reconstruction of supercontinents (Halls, 1987; Halls et al., 2000; Park et al., 1995), plume tectonics (e.g. Ernst et al., 1995; Hanski et al. 2006) and in studies of the rotation of cratonic blocks (Halls and Zhang, 2003; Halls et al., 2000). There are more than 100 giant mafic dyke swarms that extend for more than 300 km on planet Earth; thus far, the largest recognised is the Mackenzie swarm of the northern Canadian Shield, which extends for circa 2000 km (Ernst and Buchan, 2001). Mafic dykes can provide valuable information about the Mesozoic lithospheric evolution beneath the NCC (Liu et al., 2004, 2006, 2008a, b, 2009). In addition, the mafic dykes could be the key to the petrogenesis of an overall magmatic event as they may preserve different and sometimes more primitive magma compositions, less affected by assimilation (Peng, 2010). At the same time, mafic dyke swarms also provide a powerful tool in reconstructing ancient continental palaeogeography because of their large areal extent, well-defined and often short duration, palaeomagnetic record and inherent geometry (Peng, 2010). However, after their emplacement, dyke swarms may have been overprinted by later tectonothermal events resulting in deformation, metamorphism, displacement and dismemberment, and thus reconstruction is necessary prior to interpretation (Peng, 2010).

The **NCC** is composed of three Archaean tectonic units: the Eastern Continent (EC, >2500 Ma), the Western Continent (WC, >2500 Ma), and the Central Continent (CC) (Fig. 1) (Kusky and Li, 2003; Li et al., 2001; Zhao et al., 2002). Precambrian mafic dykes are widespread

* Corresponding author. Tel.: +86 851 5891962; fax: +86 851 5891664.
E-mail address: liushen@vip.gyig.ac.cn (S. Liu).

0024-4937/$ – see front matter © 2012 Elsevier B.V. All rights reserved.
doi:10.1016/j.lithos.2012.01.002

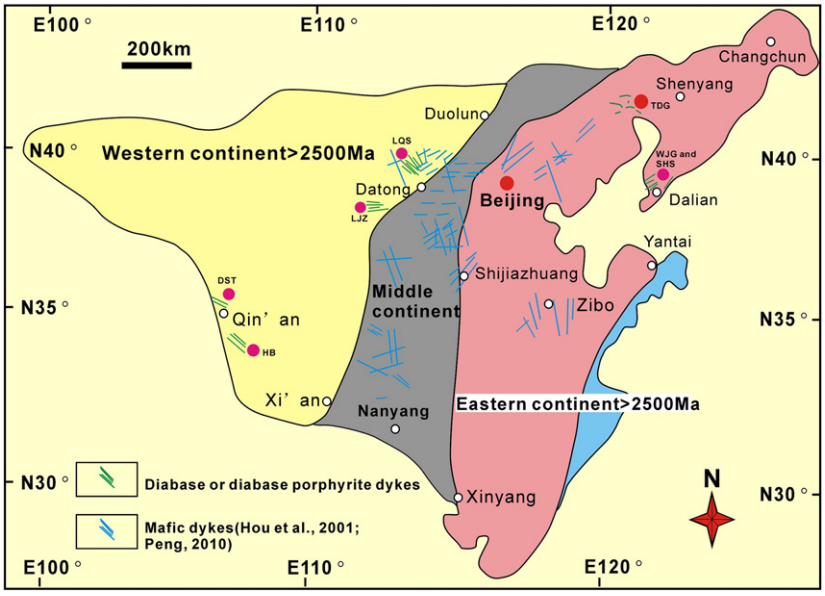

Fig. 1. Geological map of the study area, showing the three tectonic subdivisions and the distribution of the mafic dykes in the North China Craton (NCC).

throughout the NCC; occurring mainly as NE-NW-WE trending swarms (Fig. 1). Many studies have focused on the distribution of mafic dyke swarms in the NCC (Chen and Shi, 1983,1994; Chen et al., 1992; Hou et al., 2006; John et al., 2010; Li et al., 2010, 2004, 2006, 2008a, b, 2009; Peng, 2010; Peng et al., 2005, 2007, 2008, 2010, 2011a, b; Qian and Chen, 1987), together with their geochronology (Halls et al., 2000; Hou and Mu, 1994), geochemistry (Hou et al., 2001; Peng et al., 2004), flow structure (Hou et al., 1998, 2003), palaeomagnetism and tectonic stress field(s) (Halls et al., 2000; Hou et al., 2002). Some investigations on Precambrian mafic dykes in NCC have been carried out (e.g., Hou et al., 2001, 2002, 2006; John et al., 2010; Li et al., 2010; Peng et al., 2005, 2007, 2008, 2010, 2011a, b). However, systematic geochronological, geochemical and isotopic investigations of all the Precambrian mafic dyke swarms occurring across the NCC has not yet been completed and this is needed to gain a better understanding of the lithospheric mantle beneath the NCC.

During this study, we have sampled a selection of mafic dykes distributed across the Liaoning, Shanxi and Gansu provinces of the NCC in order to perform a detailed study of their geochronology and geochemistry. We present here new LA-ICP-MS zircon U–Pb ages, petrography, major and trace elemental and Sr–Nd isotopic data for the mafic dykes in these regions. The aims of this study were to: (1) constrain the formation age(s) of the mafic dykes; (2) decipher their petrogenesis, and (3) utilise this data to help better understand the evolution of the lithospheric mantle beneath the NCC.

2. Geological background and petrology

The NCC, also known as the Sino–Korean Craton, formed as a result of amalgamation of Archaean blocks either in the late Palaeoproterozoic (ca. 1.85 Ga; e.g., Guo et al., 2005; Kroöner et al., 2005; Wilde et al., 2002; Zhao et al., 2001, 2005), or alternatively in the latest Archaean (ca. 2.5 Ga), followed by Palaeoproterozoic remobilisation and recratonisation (e.g. rifting, collision and/or uplift) (Kusky and Li, 2003; Kusky et al., 2007; Li et al., 2000, 2002; Peng, 2010; Zhai and Liu, 2003; Zhai and Peng, 2007; Zhai et al., 2000). There occur more than 80 Precambrian mafic dykes in the NCC (Peng, 2010; Fig. 1); each of these dykes may provide important insights into the tectonothermal evolution of the Precambrian lithosphere of the NCC, and the possible palaeo-linkage(s) between the NCC and other craton (s). Many precise ages for the Precambrian mafic dyke swarms in the NCC have been published in recent papers (Hou et al., 2001, 2006; John et al., 2010; Li et al., 2010; Peng, 2010; Peng et al., 2005, 2007, 2008, 2010, 2011a, b), i.e., the ~0.8 Ga Zuoquan mafic dyke swarm, the 0.92 Ga Dashigou mafic dyke swarm, the 1.15 Ga Laiwu mafic dykes, the 1.62 Ga Taishan–Miyun mafic dykes, the 1.76 Ga Beitai mafic dykes, the 1.78 Ga Taihang–Lvliang mafic dykes, 1.97 Ga Xiwangshan mafic dykes, 2.15 Ga Hengling mafic dyke swarm, and the 2.5 Ga Taipingzhai–Naoyumen mafic dyke swarm.

The study area is located within the Liaoning, Shanxi and Gansu provinces, in the northern and western parts of the NCC (supplemental table). The mafic dykes (SHS-4, −5, −6; tdg-1, −2, −3) from Liaoning Province, the mafic dykes (LJZ-2, −3, −4; LQS-2, −4, −5) from Shanxi Province, and the mafic dykes (HB-2, −3, −4; WJG-5, −6, −7; DST-1, −2, −5, −7) from Gansu and Liaoning provinces are herein investigated. We describe each suite in turn.

2.1. The mafic dykes from Liaoning Province

The mafic dikes from Liaoning province intruded into Archean stratum (Fig. 2a). The individual mafic dykes are vertical and EW-trending approximately 300–600 m wide and 6.0–22 km in length. Representative photomicrographs of the mafic dykes from the NCC are provided in Fig. 3. The dykes are all dolerite with a typical doleritic texture or intergrown plagioclase and clinopyroxene (Fig. 3). The dykes are characterised by ~35–40% of micro- (0.6–1.3 mm) phenocrysts of clinopyroxene (2.0–5.5 mm), and lath-shaped plagioclase (2.5–4.5 mm) within a 60–65% matrix of clinopyroxene (0.06–0.08 mm), plagioclase (0.02–0.05 mm), and minor magnetite (~0.03–0.05 mm) and chlorite (0.04–0.06 mm). Accessory minerals include zircon and apatite.

2.2. The mafic dykes from Shanxi Province

The mafic dykes from Shanxi Province intruded into Archaean stratum (e.g., gneiss) (Fig. 2c and d). These mafic dykes are vertical and NW-trending, approximately 160–1200 m wide and 3.5–15 km in length. The dykes are all dolerite, with typical doleritic textures (Fig. 3), that mainly contain 35–38% medium-grained phenocrysts of clinopyroxene (2.0–6.0 mm) and lath-shaped plagioclase (2.5–5.0 mm) within a 60–63% matrix of clinopyroxene (0.05–0.07 mm), plagioclase (0.02–0.06 mm), and minor magnetite (~0.03–0.04 mm) and chlorite (0.04–0.07 mm). Accessory minerals include zircon and apatite.

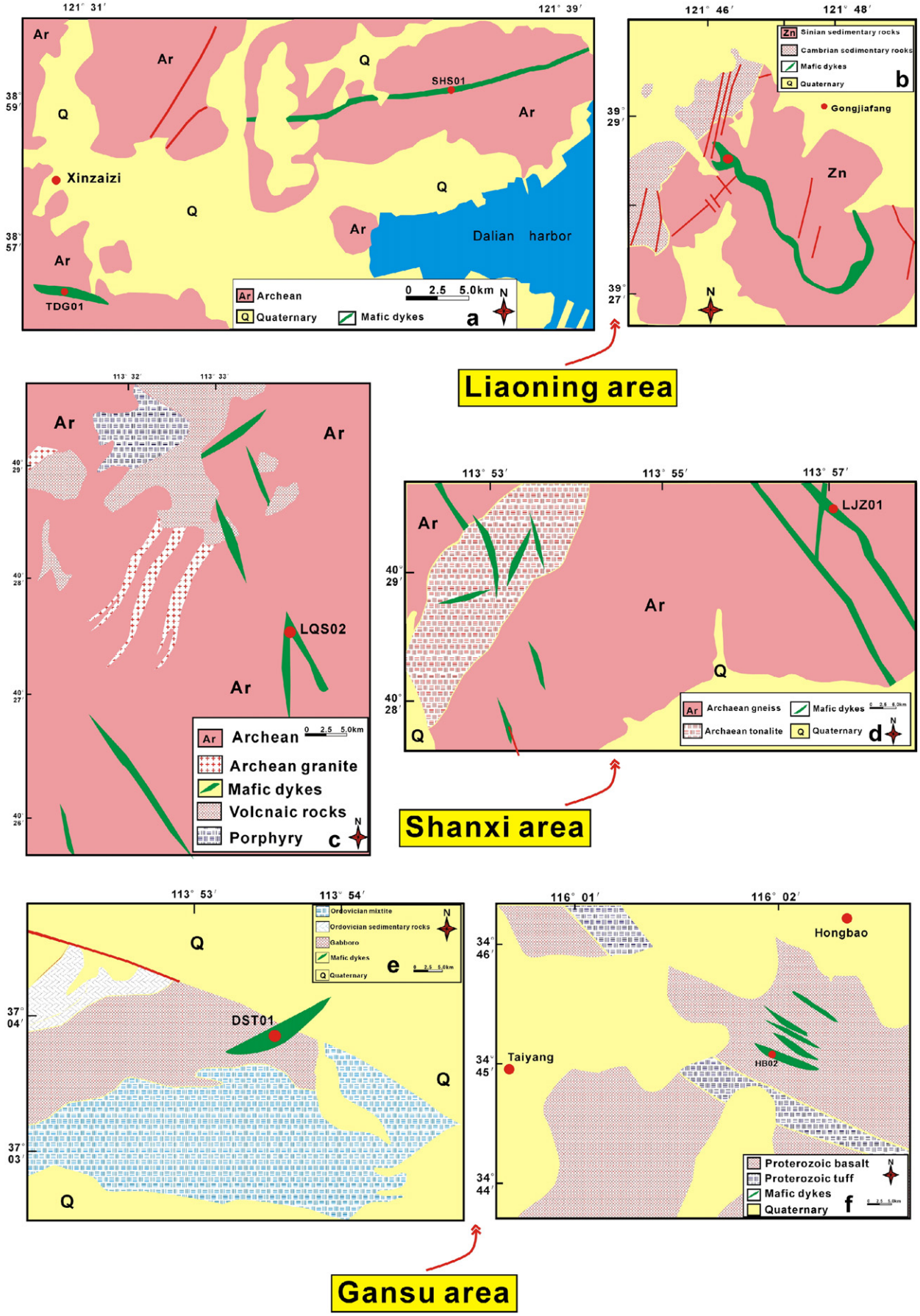

Fig. 2. Small-scale local maps for the mafic dykes from different provinces within the NCC.

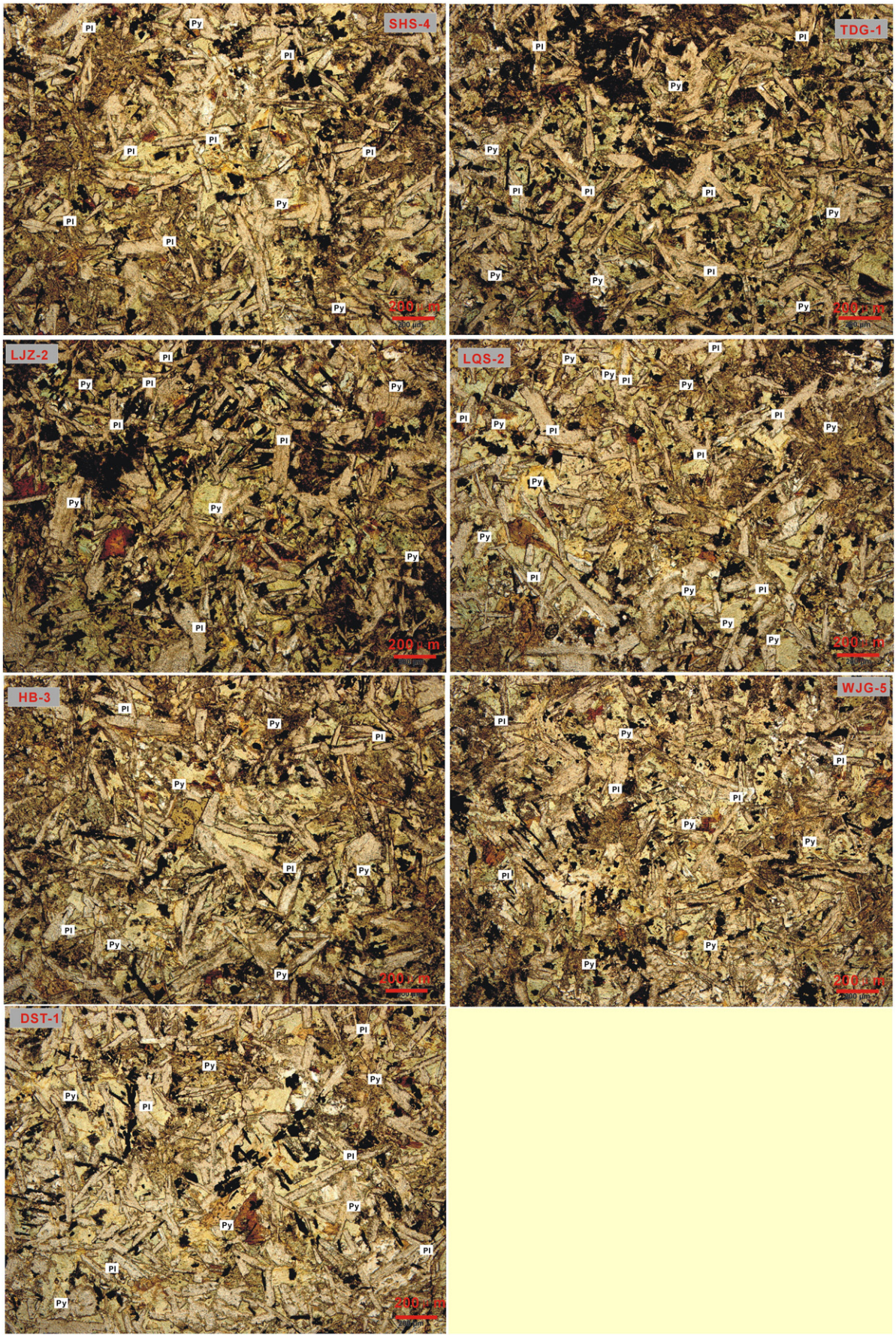

Fig. 3. Representative photomicrographs showing the petrographic features of the mafic dykes from the NCC. The samples all display doleritic textures and hence are termed dolerite dykes. Key: Py — pyroxene; Pl — Plagioclase.

2.3. The mafic dykes from Gansu and Liaoning province

The Gansu and Liaoning mafic dyke swarms intrude Sinian sedimentary rocks, Precambrian lithologies (e.g., gabbro) and Proterozoic tuff (Fig. 2b, e and f). These mafic dykes are vertical and NE-SW-trending approximately 0.8–3.0 m wide and 8.0–15 km in length. Representative photomicrographs of these dykes are provided in Fig. 3, showing again that they are dolerite, comprising 35–40% medium-grained phenocrysts of clinopyroxene (2.0–5.5 mm) and plagioclase (2.5–6.0 mm), within a 60–65% matrix of clinopyroxene (0.05–0.08 mm), plagioclase (0.02–0.05 mm), and minor magnetite (~0.03–0.05 mm) and chlorite (0.04–0.08 mm). Accessory minerals include zircon and apatite.

3. Analytical methods

3.1. U–Pb dating by LA-ICP-MS

Zircon was separated from eight samples (SHS01, TDG01, LJZ01, LQS02, HB02, WJG01 and DST01) using conventional heavy-liquid and magnetic techniques at the Langfang Regional Geological Survey, Hebei Province, China. Zircon separates were examined under transmitted and reflected light, and by cathodoluminescence petrography (CL) at the State Key Laboratory of Continental Dynamics, Northwest University, China, to reveal their external and internal structures.

Laser-ablation techniques were employed for zircon age determinations (Supplemental table; Fig. 4) using an Agilent 7500a ICP-MS instrument equipped with a 193 nm excimer laser, housed at the State Key Laboratory of Geological Processes and Mineral Resources, China University of Geoscience, Wuhan, China. Zircon # 91500 was used as a standard and NIST 610 was used to optimise the results. A spot diameter of 24 μm was used. Prior to LA-ICP-MS zircon U–Pb dating, the surfaces of the grain mounts were washed in dilute HNO_3 and pure alcohol to remove any potential lead contamination. The analytical methodology is described in detail by Yuan et al. (2004). Correction for common Pb was made following Andersen (2002). Data were processed using the GLITTER and ISOPLOT programmes (Ludwig, 2003) (supplemental table; Fig. 4). Errors for individual analyses by LA-ICP-MS are quoted at the 95% (1σ) confidence level.

3.2. Whole-rock major and trace elements, and Sr–Nd isotopes

Twenty-two samples were collected for analyses of whole-rock major and trace elements, and fifteen samples for Sr–Nd isotopes. Samples were trimmed to remove altered surfaces, cleaned with deionized water, crushed, and powdered in an agate mill.

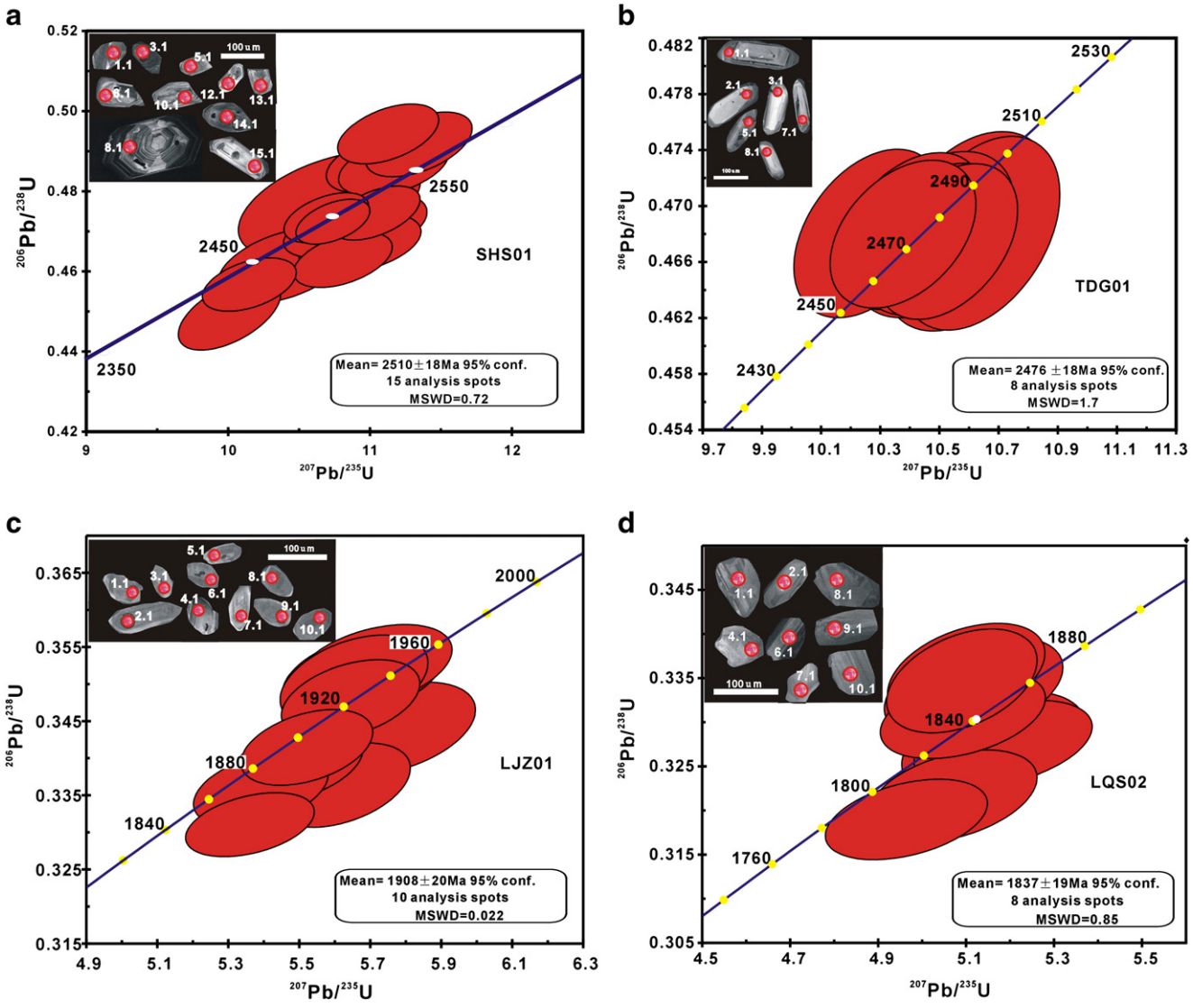

Fig. 4. LA-ICP-MS zircon U–Pb concordia diagrams for the investigated mafic dykes from the NCC.

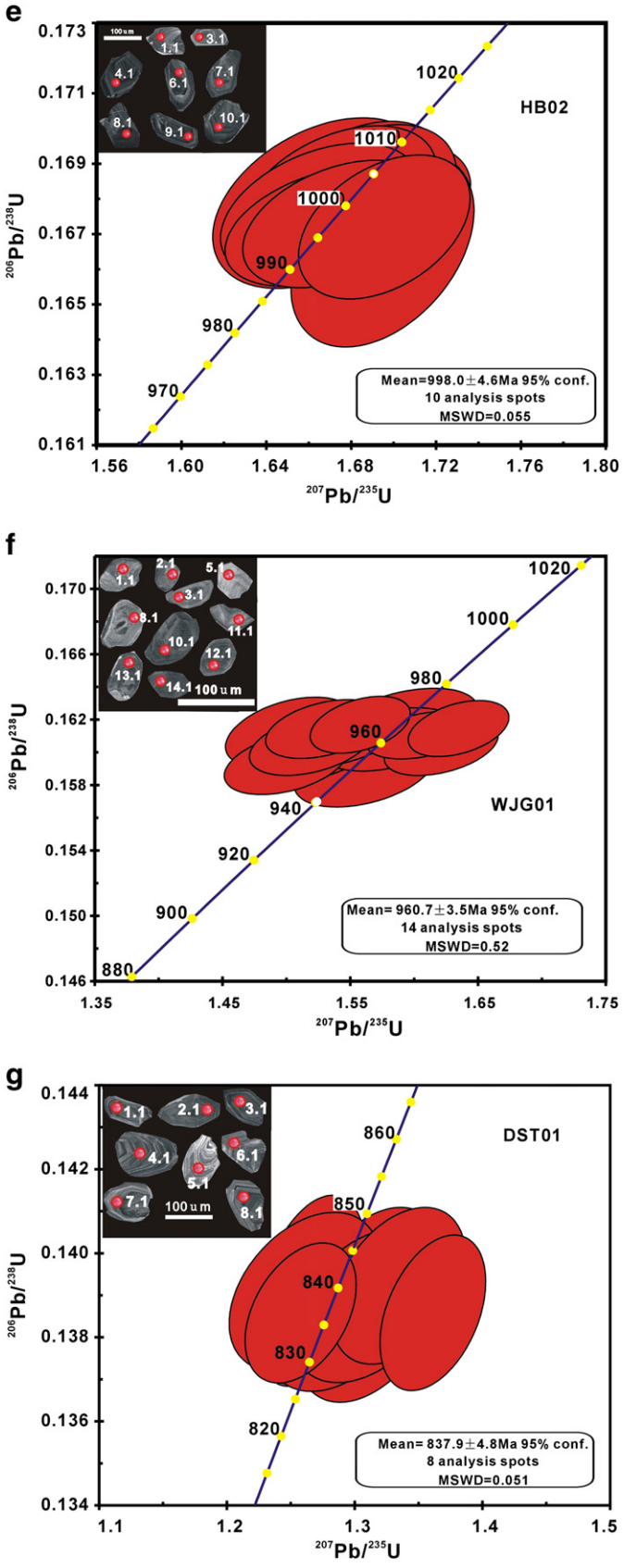

Fig. 4 (*continued*).

Major elements were analysed with a PANanalytical Axios-advance (Axios PW4400) X-ray fluorescence spectrometer (XRF) at the State Key Laboratory of Ore Deposit Geochemistry, Institute of Geochemistry, Chinese Academy of Sciences (CAS), Guiyang. Fused glass discs were prepared for analysis of the major elements. Analytical precision, as determined for the Chinese National Standards GSR-1 and GSR-3, was better than 5% for all elements (Table 1). Loss on ignition (LOI) was obtained using 1 g of powder heated to 1100 °C for 1 h.

Trace elements were measured using a Perkin–Elmer Sciex ELAN 6000 ICP-MS at the State Key Laboratory of Ore Deposit Geochemistry, Institute of Geochemistry, CAS, Guiyang. Powdered samples (50 mg) were dissolved in high-pressure Teflon bombs using a HF + HNO_3 mixture and heated for 48 h at ~190 °C (Qi et al., 2000). Rh was used as an internal standard to monitor signal drift during counting. Analyses of the international standard GBPG-1 indicated a precision generally better than 5% for all elements. Analyses of the international standards OU-6 and GBPG-1 were in close agreement with recommended values (Table 1).

For analyses of Rb–Sr and Sm–Nd isotopes, sample powders were spiked with mixed isotope tracers, dissolved in Teflon capsules with HF + HNO_3 acids, and separated by conventional cation-exchange techniques. Isotopic measurements were performed on a Finnigan Triton Ti thermal ionisation mass spectrometer (TIMS) at the State Key Laboratory of Geological Processes and Mineral Resources, China University of Geosciences, Wuhan, China. Procedural blanks were <200 pg for Sm and Nd, and <500 pg for Rb and Sr. Mass fractionation corrections for Sr and Nd isotopic ratios were based on $^{86}Sr/^{88}Sr = 0.1194$ and $^{146}Nd/^{144}Nd = 0.7219$, respectively. Analyses of standards during the period of analysis yielded the following results: NBS987 gave $^{87}Sr/^{86}Sr = 0.710246 \pm 16$ (2σ) and La Jolla gave $^{143}Nd/^{144}Nd = 0.511863 \pm 8$ (2σ). The analytical results for Sr–Nd isotopes are presented in Table 1.

4. Results

4.1. LA-ICP-MS U–Pb age determinations

Euhedral zircon grains in samples SHS01, TDG01, LJZ01, LQS02, HB02, WJG01 and DST01 are euhedral, colourless, clean and prismatic, and ranged up to 100 μm in diameter, with magmatic oscillatory zoning-a typical feature of magmatic zircon. In addition, the studied zircons all have relatively high Th/U ratios (0.4–3.5), suggestive of a magmatic origin. On the basis of CL and Th/U ratios, an igneous origin for the zircons is evident.

Fifteen grains gave a weighted mean $^{206}Pb/^{238}U$ age of 2510 ± 18 Ma (2σ) (95% confidence interval) for SHS01 (supplemental table; Fig. 4a), 8 grains provided a weighted mean $^{206}Pb/^{238}U$ age of 2476 ± 18 Ma (2σ) (95% confidence interval) for TDG01 (supplemental table; Fig. 4b), 10 grains gave a weighted mean $^{206}Pb/^{238}U$ age of 1908 ± 20 Ma (2σ) (95% confidence interval) for LJZ01 (supplemental table; Fig. 4c), 8 grains gave a weighted mean $^{206}Pb/^{238}U$ age of 1837 ± 18 Ma (2σ) (95% confidence interval) for LQS02 (supplemental table; Fig. 4d), 10 grains gave a weighted mean $^{206}Pb/^{238}U$ age of 998 ± 4.6 Ma (2σ) (95% confidence interval) for HB02 (supplemental table; Fig. 4e), 14 grains yielded a weighted mean $^{206}Pb/^{238}U$ age of 960.7 ± 3.5 Ma (2σ) (95% confidence interval) for WJG01 (supplemental table; Fig. 4f), and 8 grains gave a weighted mean $^{206}Pb/^{238}U$ age of 837.9 ± 4.8 Ma (2σ) (95% confidence interval) for DST01 (supplemental table; Fig. 4g). These determinations are the best estimates of the crystallisation ages of the mafic dykes. In addition, these have no inherited zircon characteristics. Based on the above, the mafic dykes in this study can be divided into three groups, such as: ~2.4–2.5 Ga (Fig. 4a, b), ~1.8–1.9 Ga (Fig. 4c, d) and ~0.8–1.0 Ga (Fig. 4e–g).

4.2. Major and trace elements

Table 1 shows representative whole-rock major and trace element data for the studied NCC mafic dykes.

Table 1
The major (wt.%) and trace elements (ppm) compositions of the mafic dykes in NCC.

Sample names														
Oxides and trace elements	Rock type	SiO_2	Al_2O_3	Fe_2O_3	MgO	CaO	Na_2O	K_2O	MnO	P_2O_5	TiO_2	LOI	Total	Mg #
SHS-4	diabase	53.18	13.66	8.67	10.84	3.88	1.35	1.97	0.11	0.20	0.84	6.02	100.72	73
SHS-5	diabase	52.99	13.68	9.13	11.02	3.95	1.29	1.98	0.12	0.20	0.84	6.02	100.81	73
SHS-6	diabase	52.90	13.60	8.57	10.94	4.03	1.26	2.08	0.10	0.20	0.84	5.95	100.47	74
TDG-1	diabase	50.18	13.61	15.19	5.47	6.69	3.00	1.65	0.22	0.30	2.92	1.58	100.82	44
TDG-2	diabase	49.83	13.61	14.92	5.43	6.34	3.08	1.71	0.22	0.31	2.96	2.16	100.56	44
TDG-3	diabase	49.98	13.57	14.64	5.48	7.17	3.15	1.58	0.21	0.31	2.94	1.92	100.95	45
LJZ-2	diabase	48.46	12.89	18.01	5.94	9.61	1.98	0.68	0.24	0.16	2.06	0.81	100.84	42
LJZ-3	diabase	47.76	12.85	15.87	6.34	9.74	2.08	0.65	0.23	0.14	1.65	1.86	99.17	47
LJZ-4	diabase	48.41	13.33	14.82	6.48	9.63	2.46	0.62	0.22	0.12	1.41	1.76	99.26	49
LQS-2	diabase	49.73	14.40	13.69	7.46	11.07	3.01	0.65	0.21	0.07	0.83	0.81	101.93	55
LQS-4	diabase	49.18	14.12	13.65	7.30	10.91	2.87	0.50	0.21	0.07	0.84	1.18	100.82	54
LQS-5	diabase	48.10	14.66	13.76	7.61	10.22	3.28	0.65	0.21	0.08	0.87	1.18	100.61	55
HB-2	diabase	53.21	14.24	13.18	3.8	7.22	3.94	0.39	0.23	0.27	1.93	2.35	100.75	39
HB-3	diabase	52.99	14.19	12.42	3.26	5.86	4.50	0.42	0.19	0.32	1.94	2.43	98.52	37
HB-4	diabase	52.21	13.94	12.78	3.39	7.01	4.10	0.32	0.21	0.38	1.97	2.55	98.85	37
WJG-5	diabase	49.32	13.58	15.09	5.52	7.10	2.68	1.91	0.21	0.30	2.91	2.22	100.84	45
WJG-6	diabase	49.51	13.42	15.15	5.39	7.25	2.99	1.47	0.21	0.31	2.97	2.14	100.82	44
WJG-7	diabase	49.41	13.47	15.20	5.31	7.55	3.00	1.35	0.21	0.31	2.96	2.02	100.79	43
DST-1	diabase	50.04	14.12	10.81	6.62	8.26	5.92	0.19	0.20	0.10	1.49	2.83	100.58	57
DST-2	diabase	51.02	15.26	11.12	6.21	8.26	4.30	0.16	0.20	0.10	1.49	2.76	100.87	55
DST-5	diabase	50.19	14.92	10.53	6.37	9.41	4.94	0.38	0.19	0.09	1.42	2.16	100.60	59
DST-7	diabase	49.38	15.07	11.07	6.79	8.98	4.04	0.27	0.21	0.10	1.49	3.49	100.88	61
GSR-3/RV*		44.64	13.83	13.4	7.77	8.81	3.38	2.32	0.17	0.95	2.37	2.24	99.88	
GSR-3/MV*		44.75	14.14	13.35	7.74	8.82	3.18	2.30	0.16	0.97	2.36	2.12	99.89	
GSR-1/RV*		72.83	13.4	2.14	0.42	1.55	3.13	5.01	0.06	0.09	0.29	0.70	99.62	
GSR-1/MV*		72.65	13.52	2.18	0.46	1.56	3.15	5.03	0.06	0.11	0.29	0.69	99.70	

Sample names

Oxides and trace elements	OU-6(RV*)	GBPG-1(RV*)	OU-6(MV*)	GBPG-1(MV*)	SHS-4	SHS-5	SHS-6	TDG-1	TDG-2	TDG-3	LJZ-2	LJZ-3	LJZ-4	LQS-2	LQS-4	LQS-5	HB-2	HB-3	HB-4	WJG-5	WJG-6	WJG-7	DST-1	DST-2	DST-5	DST-7
Sc	22.1	13.9	23.0	13.8	20.0	21.1	19.3	33.9	36.2	35.3	51.1	51.9	50.2	42.7	42.2	44.9	35.3	27.5	27.7	32.5	34.8	35.1	31.6	30.3	34.2	36.3
V	129	96.5	123	96.0	155	163	152	405	356	350	406	352	403	269	265	276	115	274	277	402	399	419	297	186	283	323
Cr	70.8	181	70.5	179	422	456	439	148	163	156	120	149	132	127	119	133	6.67	4.29	3.99	155	157	154	78.4	66.8	94.1	106
Ni	39.8	59.6	40.0	57.2	187	194	179	57.9	64.0	60.1	64.8	66.9	64.1	59.8	56.5	67.1	5.09	3.20	3.06	61.8	64.9	57.0	46.0	39.8	51.7	69.8
Rb	120	56.2	117	57.5	45.9	48.2	43.7	59.9	60.9	57.0	17.9	22.7	17.5	7.81	5.35	15.4	14.4	6.9	11.1	56.3	56.4	50.4	1.94	2.09	6.54	5.06
Sr	131	364	128	365	159	152	140	475	474	393	138	142	142	148	145	174	305	233	281	470	517	473	304	269	375	352
Y	27.4	18.0	27.2	19.3	18.6	19.9	19.5	37.4	42.1	39.5	37.6	34.4	31.7	20.3	20.1	20.7	52.2	51.8	48.3	44.7	43.8	40.6	33.9	33.0	30.1	31.7
Zr	174	232	169	251	128	133	118	153	165	166	117	106	85.7	24.3	24.2	41.4	172	170	149	155	160	164	98.9	96.3	91.7	97.3
Nb	14.8	9.9	14.7	10.1	6.87	6.92	5.96	16.4	16.8	16.9	6.53	5.52	4.82	2.82	2.59	2.73	4.76	4.87	4.54	16.3	16.9	16.8	0.91	0.88	0.98	
Ba	477	908	480	915	476	503	474	821	1350	1177	207	479	278	94.6	97.3	162	254	272	170	1572	1280	1099	113	110	167	176
La	33.0	53.0	32.6	54.0	24.4	26.6	25.8	16.1	17.9	17.6	12.4	10.6	9.62	5.36	4.64	4.75	17.6	16.8	15.1	18.3	18.8	17.2	3.23	3.27	2.82	2.97
Ce	74.4	103.2	79.1	94.7	46.5	50.7	50.2	34.9	39.0	37.5	25.8	23.2	20.2	11.3	9.8	10.1	40.1	40.1	38.9	36.0	39.6	36.5	10.2	10.4	9.32	9.80
Pr	7.80	11.5	7.71	12.0	5.53	6.11	6.03	4.91	5.38	5.28	3.99	3.57	3.27	1.82	1.66	1.73	5.68	5.72	5.71	5.40	5.66	5.09	1.76	1.74	1.62	1.65
Nd	29.0	43.3	29.9	44.2	24.5	25.8	24.4	24.0	26.1	25.1	17.2	16.1	14.5	8.03	7.16	7.62	26.9	27.3	27.5	25.6	25.8	24.8	10.1	9.93	8.82	9.08
Sm	5.92	6.79	5.79	7.06	4.68	4.97	4.78	6.10	6.13	6.43	5.2	4.88	4.48	2.41	2.23	2.61	7.22	7.47	7.34	6.50	6.67	6.04	3.61	3.38	3.01	3.19
Eu	1.36	1.79	1.34	1.82	1.32	1.46	1.41	2.14	2.25	2.19	1.72	1.61	1.43	1.02	1.05	1.08	2.64	2.57	2.58	2.26	2.09	2.18	1.26	1.32	1.16	1.23
Gd	5.27	4.74	5.20	4.89	4.31	4.46	4.42	6.72	7.34	6.83	6.33	5.81	5.13	3.73	3.65	3.70	8.37	8.27	8.45	7.90	7.60	7.20	4.42	4.36	4.32	4.55
Tb	0.85	0.60	0.84	0.65	0.60	0.63	0.66	1.10	1.14	1.06	1.08	0.95	0.87	0.57	0.55	0.55	1.37	1.40	1.35	1.20	1.13	1.05	0.84	0.78	0.77	0.78
Dy	4.99	3.26	4.98	3.33	3.52	3.71	3.69	6.57	7.16	6.73	7.24	6.44	5.55	3.93	3.64	4.04	9.34	9.71	8.96	7.46	7.39	6.67	6.04	5.71	4.93	5.06
Ho	1.01	0.69	1.04	0.67	0.70	0.77	0.77	1.32	1.41	1.35	1.54	1.29	1.23	0.87	0.84	0.90	2.03	2.04	1.94	1.52	1.37	1.36	1.30	1.22	1.16	1.21
Er	2.98	2.01	2.97	2.08	1.86	2.06	2.11	3.45	3.68	3.42	4.30	3.84	3.32	2.56	2.47	2.60	5.50	5.66	5.16	4.00	3.59	3.51	3.70	3.59	3.12	3.25
Tm	0.44	0.30	0.43	0.31	0.25	0.28	0.29	0.46	0.48	0.45	0.60	0.52	0.47	0.37	0.36	0.35	0.81	0.80	0.71	0.50	0.47	0.44	0.53	0.53	0.48	0.49
Yb	3.00	2.03	2.97	2.11	1.68	1.87	1.86	2.99	3.36	3.06	3.79	3.42	3.04	2.41	2.30	2.32	5.42	5.46	4.73	3.31	3.15	3.04	3.49	3.43	2.94	3.08
Lu	0.45	0.31	0.45	0.32	0.26	0.28	0.28	0.44	0.49	0.48	0.56	0.49	0.51	0.35	0.37	0.37	0.79	0.79	0.71	0.48	0.50	0.45	0.53	0.49	0.43	0.46
Hf	4.70	6.07	4.68	6.12	3.38	3.64	3.13	3.90	4.29	4.25	3.24	2.80	2.35	1.05	0.95	1.34	4.93	4.82	4.28	4.12	4.30	4.20	2.75	3.02	2.38	2.53
Ta	1.06	0.40	1.11	0.42	0.43	0.44	0.40	1.09	1.15	1.11	0.57	0.34	0.35	0.23	0.20	0.22	0.37	0.35	0.36	1.07	1.10	1.09	0.08	0.08	0.08	0.08
Pb	28.2	14.1	32.3	13.4	12.4	12.2	11.3	21.4	12.0	9.60	3.70	2.53	2.83	3.70	1.41	1.87	1.86	1.82	1.69	14.3	10.0	12.5	0.38	0.44	0.88	1.91
Th	11.5	11.2	11.2	12.0	3.97	4.13	4.04	2.61	2.90	2.90	1.78	1.55	1.44	0.49	0.37	0.47	2.47	2.43	2.30	2.58	2.81	2.74	0.30	0.28	0.25	0.27
U	1.96	0.90	1.97	0.91	0.87	0.86	0.85	0.55	0.62	0.61	0.51	0.38	0.35	0.10	0.07	0.11	0.69	0.48	0.42	0.48	0.59	0.58	0.10	0.09	0.09	0.08
(La/Yb)N					10.4	10.2	9.93	3.86	3.83	4.13	2.35	2.22	2.27	1.60	1.45	1.47	2.33	2.20	2.30	3.96	4.27	4.05	0.66	0.69	0.69	0.69
dEu					0.94	0.99	1.00	1.35	0.97	0.95	0.85	1.07	1.13	1.21	0.77	0.82	1.08	1.28	1.12	1.07	0.95	0.92	0.93	0.99	1.03	0.97

RV*: recommended values; MV*: measured values.

Table 2
Sr–Nd isotopic compositions of the mafic dykes in NCC.

Sample	Age(Ma)	Sm(ppm)	Nd(ppm)	Rb(ppm)	Sr(ppm)	$^{87}Rb/^{86}Sr$	$^{87}Sr/^{86}Sr$	2σ	$(^{87}Sr/^{86}Sr)_i$	$^{147}Sm/^{144}Nd$	$^{143}Nd/^{144}Nd$	2σ	$(^{143}Nd/^{144}Nd)_i$	$\varepsilon_{Nd}(t)$
SHS-4	2510	4.68	24.5	45.9	159	0.8356	0.705266	10	0.674947	0.1154	0.512947	10	0.510058	13.3
SHS-5		4.97	25.8	48.2	152	0.9174	0.707997	12	0.674711	0.1166	0.513242	10	0.510070	13.5
TDG-1	2476	6.10	24.0	59.9	475	0.3649	0.705065	10	0.692007	0.1538	0.511343	8	0.510099	13.2
TDG-3		6.43	25.1	57.0	393	0.4196	0.707023	8	0.692008	0.1549	0.511528	8	0.510097	13.2
LJZ-2	1908	5.20	17.2	17.9	138	0.3754	0.711997	12	0.701688	0.1828	0.511746	10	0.510761	11.6
LJZ-3		4.88	16.1	22.7	142	0.4626	0.714556	10	0.701850	0.1832	0.511985	10	0.510772	11.8
LJZ-4		4.48	14.5	17.5	142	0.3567	0.712208	10	0.702413	0.1868	0.511696	8	0.510761	11.6
LQS-2	1837	2.41	8.03	7.81	148	0.1527	0.706163	8	0.702127	0.1814	0.511179	9	0.510793	10.4
LQS-4		2.23	7.16	5.35	145	0.1068	0.704946	8	0.702124	0.1883	0.511066	10	0.510796	10.5
HB-2	998	7.22	26.9	14.4	305	0.1366	0.704844	10	0.702894	0.1626	0.511961	8	0.511774	8.3
HB-3		7.47	27.3	6.88	233	0.0856	0.704936	10	0.703715	0.1651	0.511903	10	0.511786	8.5
WJG-5	960.7	6.50	25.6	56.3	470	0.3466	0.705237	12	0.700477	0.1536	0.512237	10	0.511781	7.5
WJG-6		6.67	25.8	56.4	517	0.3160	0.705163	10	0.700823	0.1566	0.512208	9	0.511792	7.7
DST-1	837.9	3.61	10.1	1.94	304	0.0185	0.705025	8	0.704804	0.2154	0.511914	8	0.511893	6.6
DST-2		3.38	9.9	2.09	269	0.0225	0.704953	10	0.704684	0.2059	0.511917	10	0.511891	6.5

4.2.1. ~2.4–2.5 Ga mafic dykes

Mafic dykes intruded into Archaean stratum (Fig. 2a). The dykes have low SiO_2 (49–54 wt.%) and Al_2O_3 (13.5–13.7 wt.%) contents, variable Fe_2O_3 (8.5–15.2 wt.%), CaO (3.8–7.2 wt.%), TiO_2 (0.8–3.0 wt.%) and P_2O_5 (0.2–0.31 wt.%), and low to high MgO contents (5.4–11.1 wt.%), $Mg^{\#} = 44–74$, relatively low Na_2O contents (1.2–3.2 wt.%), and variable K_2O (1.5–2.1 wt.%) (Table 1). In a plot of alkalis ($Na_2O + K_2O$) versus SiO_2 (Fig. 5a), the mafic samples plot in the fields for the alkaline and sub-alkaline series. In K_2O versus SiO_2 plot (Fig. 5b), the dykes plot in the high-K calc-alkaline fields. All of the samples show highly variable contents of Sr (140–475 ppm) and Ba (474–1350 ppm), are low and variable in light rare earth elements (LREEs; e.g., $(La/Yb)_N = 0.55–0.87$), and have weak Eu anomalies ($\delta Eu = 0.94–1.35$) (Table 1; Fig. 6a). In a primitive mantle-normalised trace elemental diagram, the mafic dykes are characterised by enrichment in Ba, U, La and Pb, and depletion in Rb, Sr and high field strength elements (HFSEs; Nb, Ta, minor Ti) (Fig. 6b). The mafic dykes show regular trends of decreasing Fe_2O_3, CaO, Na_2O, P_2O_5, TiO_2, Sr, Ba and Zr with increasing

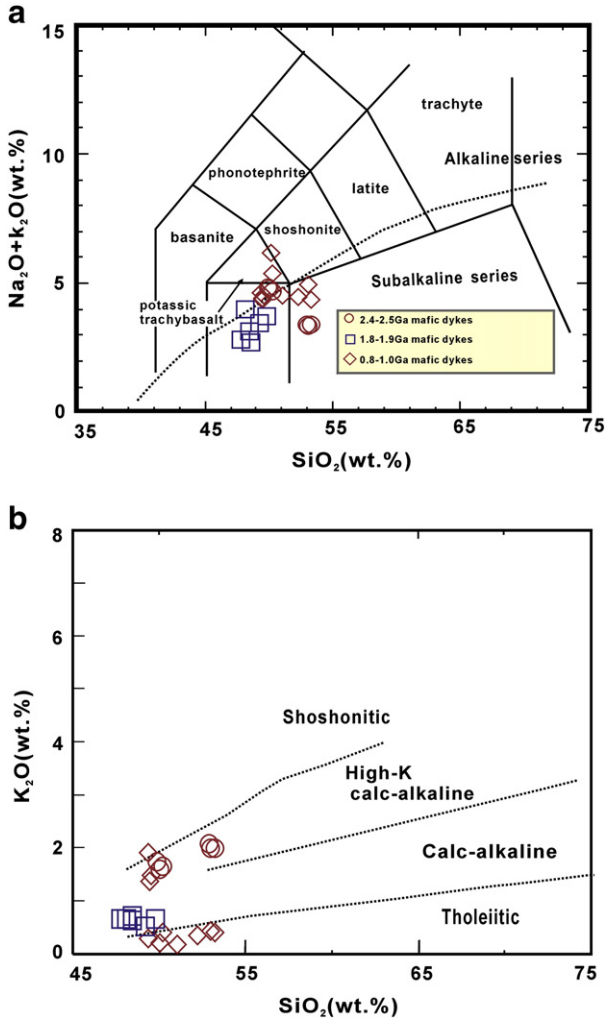

Fig. 5. Plots of: SiO_2 versus: a) $Na_2O + K_2O$ and b) K_2O for the mafic dykes from the NCC.

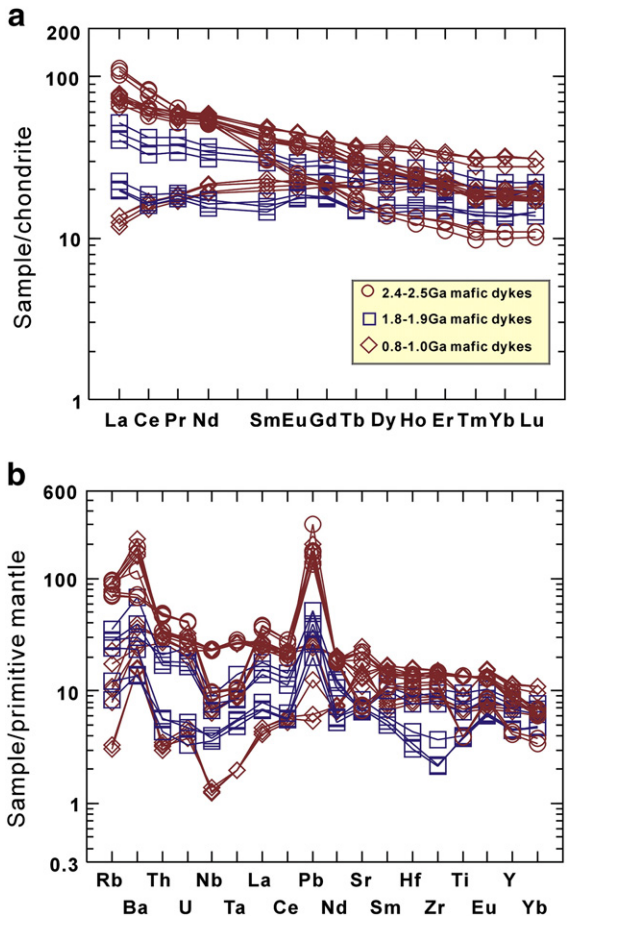

Fig.6. Chondrite-normalised rare earth element patterns and primitive mantle-normalised spider diagrams for the mafic dykes from the NCC. Primitive mantle and chondritic abundances are from Sun and McDonough (1989). Symbol keys are the same as in this Fig. 5.

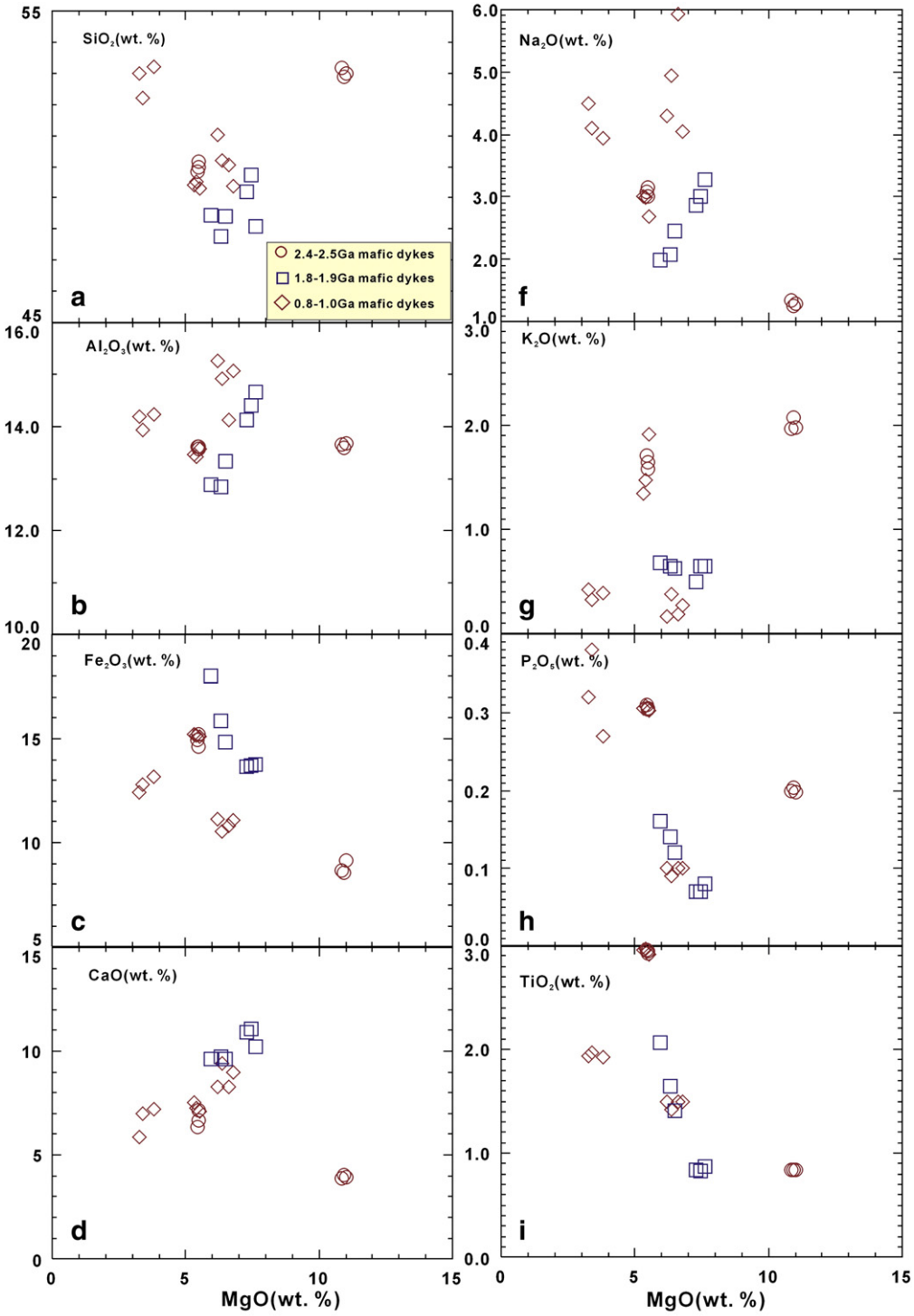

Fig. 7. Plots of MgO versus SiO_2, TiO2, Al_2O_3, Fe_2O_3, CaO, Na_2O, K_2O, P_2O_5 and TiO_2 for the studied mafic dykes from the NCC. Symbol keys are the same as in this Fig. 5.

MgO (Fig. 7c, f, h, i; Fig. 8a,d, f), increasing SiO_2, Al_2O_3, K_2O, Th, Ni and Cr with increasing MgO (Fig. 7a, b, g; Fig. 8b, c, e).

4.2.2. ~1.8–1.9 Ga mafic dykes

~1.8–1.9 Ga mafic dykes intruded into Archaean stratum (e.g., gneiss) (Fig. 2c and d). The dykes have low SiO_2 (47–50 wt.%) contents, variable Al_2O_3 (12.8–14.7 wt.%), Fe_2O_3 (13.6–18.1 wt.%), CaO (9.6–11.1 wt.%), TiO_2 (0.8–2.1 wt.%) and P_2O_5 (0.07–0.16 wt.%), and moderate MgO contents (5.9–7.6 wt.%), $Mg^{\#}$ = 42–55, relatively low Na_2O contents (1.9–3.3 wt.%), and variable K_2O (0.5–0.7 wt.%) (Table 1). In a plot of total alkalis versus SiO_2 (Fig. 5a), the mafic samples plot in the fields for the sub-alkaline series. In K_2O versus SiO_2 plot (Fig. 5b), the dykes plot in the calc-alkaline fields. All the samples show highly variable contents of Sr (138–174 ppm) and Ba (94.6–479 ppm), are low and variable in LREE's (e.g., $(La/Yb)_N$ = 1.45–2.35), and have negative and positive Eu anomalies (δEu = 0.77–1.21) (Table 1; Fig. 6a). In a primitive mantle-normalised trace elemental diagram, the mafic dykes are characterised by enrichment in Ba, La and Pb, and depletion in Rb, some Th, U and Nd, and HFSE (Nb, Ta, minor Zr, Hf, and Ti) (Fig. 6b). The mafic dykes show regular trends of decreasing Fe_2O_3, P_2O_5, TiO_2, Th and Zr with

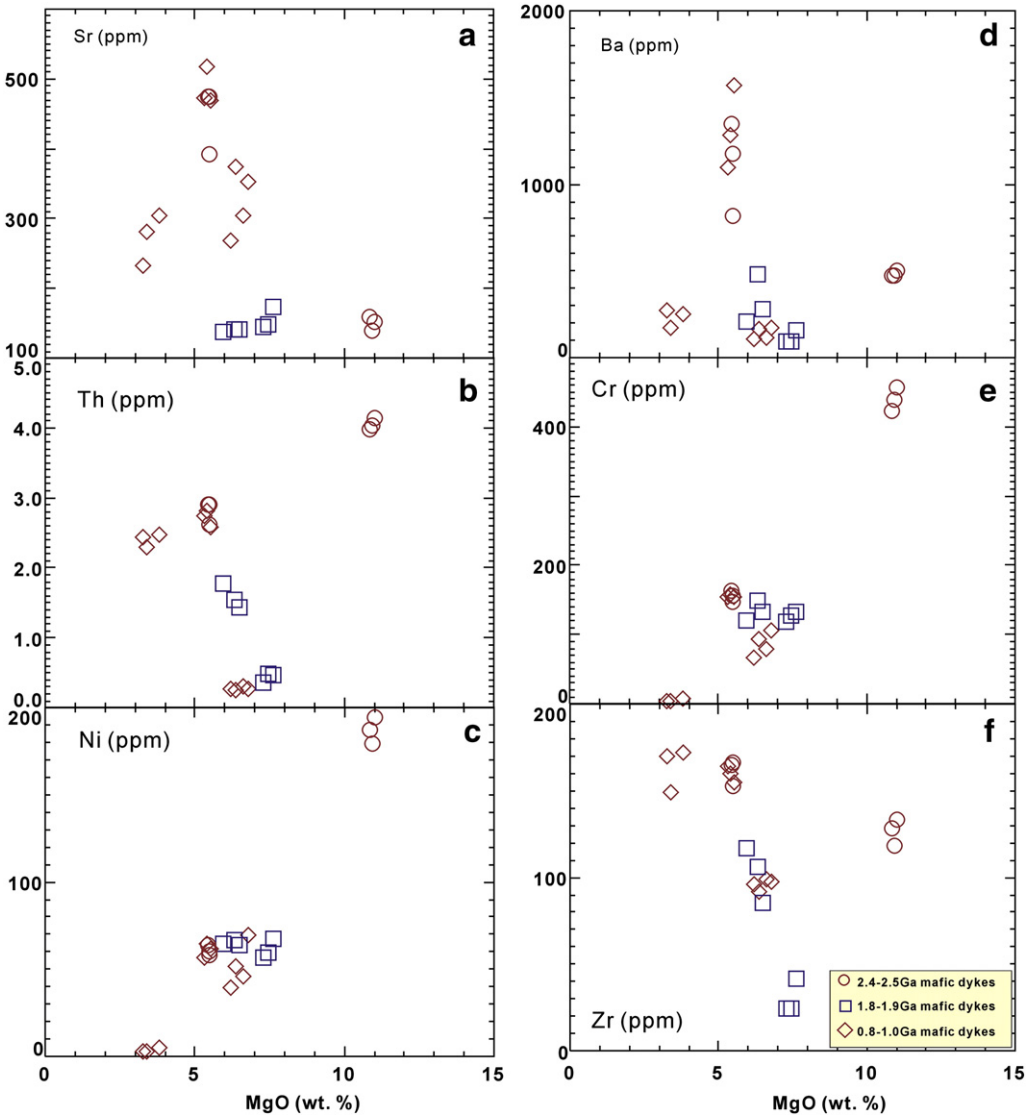

Fig. 8. Plots of MgO versus Sr, Th, Ni, Ba, Cr and Zr for the mafic dykes from the NCC.

increasing MgO (Fig. 7c, h, i; Fig. 8b, f), increasing Al_2O_3, CaO, Na_2O, and Sr with increasing MgO (Fig. 7b, d, f; Fig. 8a), and no apparent correlations between SiO_2, K_2O and Cr and MgO (Fig. 7a, g; Fig. 8e).

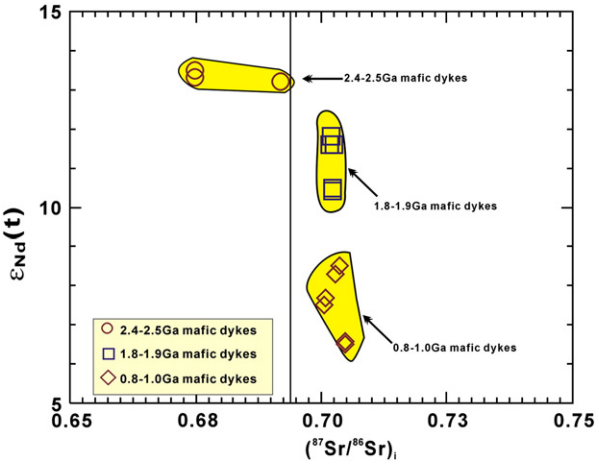

Fig. 9. Plot of $(^{87}Sr/^{86}Sr)_i$ versus ε_{Nd} (t) for the studied Precambrian mafic dyke from the NCC. Symbol keys are the same as in this Fig. 5.

4.2.3. 0.8–1.0 Ga mafic dykes

The 0.8–1.0 Ga mafic dykes intruded Sinian sedimentary rocks, Precambrian gabbro and Proterozoic tuff (Fig. 2b, e and f). These rocks have low SiO_2 contents (49–54 wt.%), variable Al_2O_3 (13.4–15.3 wt.%), Fe_2O_3 (10.5–15.2 wt.%), CaO (5.8–9.4 wt.%), TiO_2 (1.4–3.0 wt.%) and P_2O_5 (0.09–0.4 wt.%), and low to high MgO contents (3.3–6.8 wt.%), $Mg^{\#} = 37–61$, relatively low to high Na_2O contents (2.6–5.9 wt.%), and variable K_2O (0.16–1.91 wt.%) (Table 1). In a plot of $(Na_2O + K_2O)$ versus SiO_2 (Fig. 5a), the mafic samples plot in the fields for the alkaline and sub-alkaline series. In K_2O versus SiO_2 plot (Fig. 5b), the dykes plot in the Tholeiitic and high-K calc-alkaline fields. All these rocks show highly variable contents of Sr (233–517 ppm) and Ba (110–1572 ppm), are low and variable in LREE's (e.g., $(La/Yb)_N = 0.66–4.27$), and have no or positive Eu anomalies ($\delta Eu = 0.92–1.28$) (Table 1; Fig. 5a). In a primitive mantle-normalised trace elemental diagram, the mafic dykes are characterised by enrichment in Ba, U, Pb and Sr, and depletion in Rb and HFSE's (Nb, Ta and Ti) (Fig. 6b). The mafic dykes show regular trends of decreasing SiO_2, Fe_2O_3, P_2O_5, TiO_2, Th and Ba with increasing MgO (Fig. 7a, c, h, i; Fig. 8b, d), increasing Al_2O_3, CaO, TiO_2, Sr, Ni and Cr with increasing MgO (Fig. 7b, d; Fig. 8b, d, e), and no apparent correlations between Na_2O, K_2O, Ba and Zr and MgO (Fig. 7f, g; Fig. 8d and f).

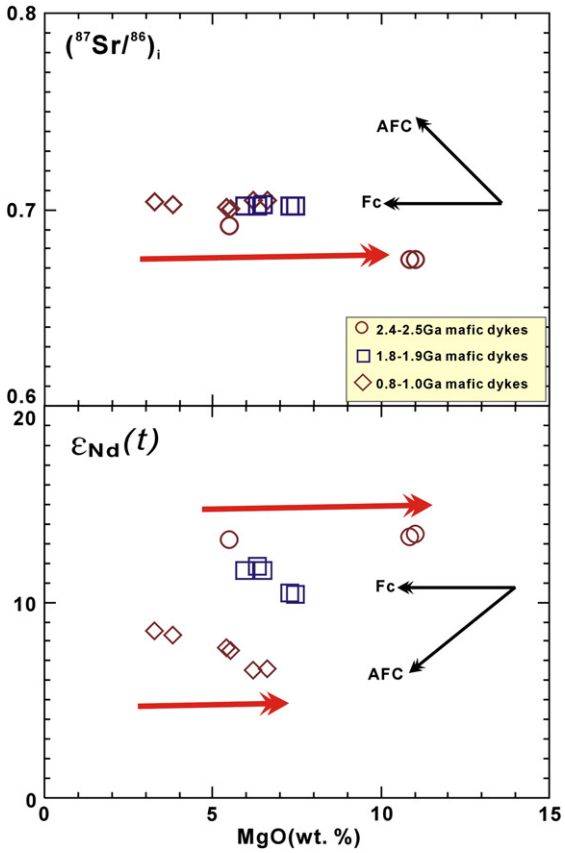

Fig. 10. Plots of MgO versus: a) the initial $^{87}Sr/^{86}Sr$ ratio and b) ε_{Nd} (t) for the studied mafic dykes from the NCC. FC: fractional crystallisation; AFC: assimilation and fractional crystallisation. Symbol keys are the same as in this Fig. 5.

4.3. Sr–Nd isotopes

4.3.1. ~2.4–2.5 Ga mafic dykes

Sr and Nd isotopic data for representative samples of the mafic dykes (Table 2; Fig. 9), yield low ranges in $(^{87}Sr/^{86}Sr)_i$ values (~2.4–2.5 Ga; 0.6747–0.6920) and relatively high initial ε_{Nd} (t) values (~2.4–2.5 Ga; 13.2–13.5), indicating a compositionally depleted mantle source.

4.3.2. ~1.8–1.9 Ga mafic dykes

Sr and Nd isotopic data for representative samples of these mafic dykes (Table 2; Fig. 9), give low ranges in $(^{87}Sr/^{86}Sr)_i$ values (~1.8–1.9 Ga; 0.7017–0.7024) and positive initial ε_{Nd} (t) values (~1.8–1.9 Ga; 10.4–11.8), indicating a compositionally depleted mantle source.

4.3.3. 0.8–1.0 Ga mafic dykes

Sr and Nd isotopic data of representative mafic dykes (Table 2; Fig. 9), show low ranges in $(^{87}Sr/^{86}Sr)_i$ values (0.8–0.9 Ga; 0.7005–0.7048) and high initial ε_{Nd} (t) values (0.8–0.9 Ga; 6.5–8.5), as well as, indicating a compositionally depleted mantle source.

5. Petrogenesis

Results from our new zircon data, geochemical and Sr–Nd isotopic compositions of three group mafic dykes, enable us to place constraints on several key issues regarding the petrogenesis (crustal contamination, fractional crystallisation and the source and genetic model) of the NCC. Thus, we discuss these issues further as follows.

5.1. Crustal contamination

In the primitive mantle normalised diagrams (Fig. 6b) all the studied mafic rocks show very distinctive negative anomalies in HFSEs (Nb, Ta and Ti), and positive anomalies in Pb. HFSE-depletion indicates the involvement of components from the proto-Tethyan oceanic or ancient continental crust (Zhang et al., 2005). In addition, the higher Ba/Nb ratios (31.7–181) in these rocks, however, are different from those of most intraplate volcanic rocks including N-MORB, OIB, alkali basalt and kimberlite with much lower Ba/Nb ratios of 20 to 1 (Jahn et al., 1999). These suggest that continental materials (granitoids, granulites, sediments, etc.) might be involved in these mantle-derived magmas. However, crustal assimilation can cause significant variations in Sr–Nd isotopes within a group of rocks, and can produce an apparent positive correlation between MgO and ε_{Nd} (t) values, and a negative correlation between MgO and $(^{87}Sr/^{86}Sr)_i$ values. These features are not observed in each group studied mafic dykes from NCC, however, indicating a general lack of crustal contamination (Fig. 10). The investigated mafic dykes are characterised by depletion in Th and U relative to La in the primitive mantle-normalised diagrams (Fig. 6b), also eliminating the possibility of significant upper-middle crustal contamination (Taylor and McLennan, 1985). In addition, the three group of mafic dykes are further characterised by relatively low contents of Nb (0.88–16.9 ppm), Zr (24.2–172 ppm), Th (0.25–4.13 ppm), and Rb (2.09–60.9 ppm) compared to upper crust (which yields typical values of Nb = 25 ppm, Zr = 190 ppm, Th = 10.5 ppm and Rb = 84 ppm; Rudnick and Fountain, 1995; Rudnick and Gao, 2003), again suggesting negligible crustal contamination. Hence, a likely alternative candidate for contamination might be lower crust; accordingly, the Sr content in the melts would decrease following magma differentiation due to the lower Sr abundance of lower crust rocks (e.g., 350 ppm, Rudnick and Fountain, 1995). However, no correlation between MgO and Sr is evident in the illustrated magma differentiation trend (Fig. 8a).

Furthermore, the lack of evident correlation between the ε_{Nd} (t) values and Nd concentrations for the studied mafic dykes likely precludes assimilation and fractional crystallisation (AFC) as a major process during their late evolutionary stages (Zhong et al., 2007), at a shallow-crustal level.

In summary, it is concluded that the geochemical and Sr–Nd isotopic signatures of the three groups of NCC mafic dykes were inherited mainly from their mantle source(s) prior to emplacement and do not reflect significant crustal assimilation. Moreover, there is no evidence that ancient continental crustal materials from the NCC were involved during magma ascent by crustal contamination or that could have affected the parental magmas to the mafic dykes, in the source region as a result of metasomatism.

5.2. Fractional crystallisation

The variable $Mg^{\#}$ (37–74) and compatible element content, such as Cr (4.29–456 ppm) and Ni (3.06–194 ppm) (Table 1) of the mafic dykes is consistent with significant fractionation. For the studied mafic dykes, MgO shows a negative correlation with SiO_2, Fe_2O_3 and TiO_2, and positive correlation with Al_2O_3 and CaO (Fig. 7a, b, c, d, i), probably related to the fractionation of olivine-, pyroxene-, hornblende, plagioclase and Fe–Ti oxides (e.g., rutile, ilmenite, titanite, etc.); plagioclase fractional crystallisation is further supported by the negative Eu and Sr anomalies observed in some of the studied mafic dykes (Fig. 6a and b).

In general, the presence of negative Nb, Ta, and Ti anomalies in the analysed samples (Fig. 6b) supports the fractionation of Fe–Ti oxides (e.g., rutile, ilmenite, and titanite) or that these magmas formed in a destructive-margin environment with a residual Ti-bearing phase (e.g., spinel) in the mantle source during partial melting.

Moreover, the mafic dykes shows decreasing Zr with increasing SiO_2 (not shown), indicating that zircon was saturated in the magma and was also a major fractionating phase (Li et al., 2007).

5.3. The source and genetic model

The studied mafic dykes are the result of lithospheric extension, with the widespread occurrence of these dykes indicating that the NCC has undergone perennial extension. Hence, a discussion of the petrogenesis of the studied mafic dykes is very important in our understanding of Precambrian extensional faulting and tectonic evolution in this region, and also the evolution of the mantle beneath the NCC. Low SiO_2 contents (47.76–53.21 wt.%; Table 1) suggest that the mafic dykes were derived from mafic mineral accumulation or an ultramafic source (Liu et al., 2008a). Crustal rocks can be ruled out as possible sources because experimental evidence shows that partial melting of any of the older, exposed crustal rocks in the area (e.g., Hirajima et al., 1990; Kato et al., 1997; Yang et al., 1993; Zhang et al., 1994, 1995) and lower crustal intermediate granulites (Gao et al., 1998) of the deep crust would produce high-Si magmas (i.e., granitoid liquids; Rapp et al., 2003). Therefore, these mafic dykes likely originated directly in the mantle.

Based on the above interpretations, the possibility of significant crustal assimilation in the genesis of the mafic magmas has also been eliminated. Therefore, we prefer the involvement of crustal components in the source. Nevertheless, it is necessary to know by which mechanism the crustal materials sank into the lithospheric mantle. One possible explanation, that has previously been proposed to account for the petrogenesis (e.g., involvement of crust) of the Precambrian mafic magmatism across the NCC, is through the subduction of the proto-Tethyan oceanic crust (Liu et al., 2009), whereby, the melts from subducted oceanic crust resulted in metasomatism and the modification of lithospheric mantle beneath the NCC. The subduction of proto-Tethyan oceanic crust could also have resulted in the extension of the continental lithosphere beneath the NCC (Liu et al., 2008a, b, 2009). Lithosphere extension then induced decompression melting of the metasomatised and modified sub-NCC lithospheric mantle, which produced all of the intense magmatism in the NCC during the Precambrian. However, the question of whether oceanic crust has contributed to the Precambrian magmatic activities of the NCC and if so when this occurred has not adequately been addressed to date. As such, these various models and ideas need to be investigated and evidence in support or against obtained before definitive conclusions can be drawn.

In addition to the above discussion, an alternative mechanism, that of foundering of continental lower crust into underlying convecting mantle has been proposed to play a role in plume magmatism, crustal evolution and the formation of chemical heterogeneities within the mantle (Anderson, 2006; Arndt and Goldstein, 1989; Elkins-Tanton, 2005; Escrig et al., 2004; Gao et al., 2004, 2008; Jull and Kelemen, 2001; Kay and Kay, 1991; Lustrino, 2005; Rudnick and Fountain, 1995). This is due to the unique chemical and physical properties of eclogite formed by high to ultra-high pressure metamorphism of basalt. Because of its higher density than that of lithospheric mantle peridotite (by some 0.2–0.4 g cm^{-3}; Anderson, 2006; Jull and Kelemen, 2001; Levander et al., 2006; Rudnick and Fountain, 1995;), eclogite can and has been recycled into the mantle (Arndt and Goldstein, 1989; Gao et al., 2004; Jull and Kelemen, 2001; Kay and Kay, 1991). On the other hand, eclogites have lower melting temperatures than mantle peridotites (Kogiso et al., 2003; Rapp et al., 1999; Sobolev et al., 2005, 2007; Yaxley, 2000; Yaxley and Green, 1998), and as foundered, silica-saturated eclogites heat up, they will produce silicic melts (e.g., tonalite to trondhjemite) that may hybridise, variably, with overlying mantle peridotite. Such reactions may produce an olivine-free pyroxenite, which, if subsequently melted, will generate basaltic melt (Gao et al., 2008; Herzberg et al., 2007; Kogiso et al., 2003; Sobolev et al., 2005, 2007). The above model is ideal in explaining both mantle metasomatism and the origin of the NCC primary magmas to the mafic dykes in our study area. Moreover, this model has been successfully used to interpret the petrogenesis of the Mesozoic mafic dykes in Shandong Province, China (Liu et al., 2008a, b, 2009).

6. Conclusions

Based on geochronological, geochemical, and Sr–Nd isotopic data, we draw the following conclusions concerning the origins of the investigated NCC mafic dykes:

(1) LA-ICP-MS U–Pb zircon age data indicate that the studied Precambrian mafic dyke swarms of the NCC were formed between 837.9 ± 4.8 Ma and 2510 ± 18 Ma. Furthermore, these mafic dykes can be divided into three groups: ~2.4–2.5 Ga, ~1.8–1.9 Ga and 0.8–1.0 Ga.

(2) The three groups of mafic dykes belong to the alkaline and sub-alkaline magma series, and show Tholeiitic, calc-alkaline and high-K calc-alkaline affinities based on their total alkali to SiO_2 (wt.%) contents. The rocks have low and variable LREE contents [$(La/Yb)_N$ = 0.66–10.4], show variable Eu anomalies (δEu = 0.76–1.35) and positive anomalies in Ba, U, La and Pb, and depleted in Rb and HFSE's (Nb, Ta, Ti and minor Zr and Hf). The mafic dykes in this study all show relatively low radiogenic Sr ($(^{87}Sr/^{86}Sr)_i$ (0.6747–0.7049) and large ε_{Nd} (t) (6.5–13.5), suggesting origination from a depleted mantle, hybridised by foundered lower crust.

(3) The studied mafic dyke swarms groups all derive from a mantle source. The parent magmas probably originated via fractional crystallisation from a basaltic magma. Fractionation [involving olivine, pyroxene, hornblende, plagioclase and Fe–Ti oxides (e.g., rutile, ilmenite, titanite, etc.)] occurred during ascent of the dykes, with negligible crustal contamination.

Supplementary materials related to this article can be found online at doi:10.1016/j.lithos.2012.01.002.

Acknowledgements

The authors would like to thank G. Nelson Eby and three anonymous reviewers for their constructive reviews. We also thank Rohini Shivaram for quick editorial handling of the manuscript. This research was supported by the National Nature Science Foundation of China (grant nos. 40773020, 40972071, 40673029, 90714010 and 40634020). We are grateful to Xiaobiao Li and Lian Zhou for assisting with the analyses of Sr and Nd isotopes, and to Yongsheng Liu and Zhaochu Hu for their help with the zircon U–Pb dating.

References

Andersen, T., 2002. Correction of common lead in U–Pb analyses that do not report ^{204}Pb. Chemical Geology 192, 59–79.
Anderson, D.A., 2006. Speculations on the nature and cause of mantle heterogeneity. Tectonophysics 146, 7–22.
Arndt, N.T., Goldstein, S.L., 1989. An open boundary between lower continental crust and mantle: its role in crust formation and crustal recycling. Tectonophysics 161, 201–212.
Chen, X.D., Shi, L.B., 1983. Primary research on the diabase dyke swarms in Wutai–Taihang area. Chinese Science Bulletin 16, 1002–1005.
Chen, X.D., Shi, L.B., 1994. Basic dyke swarms in extensional structures. In: Qian, X.L. (Ed.), Extensional structures. Geological Publishing House, Beijing, pp. 71–74.
Chen, X.D., Shi, L.B., Jia, S.F., 1992. Proterozoic basic dyke swarms in North China. Seismology and Geology 14, 351–357 (in Chinese with English abstract).
Elkins-Tanton, L.T., 2005. Continental magmatism caused by lithospheric delamination. In: Foulger, G.R., Natland, J.H., Presnall, D.C., Anderson, D.L. (Eds.), Plates, Plumes, and Paradigms: Geological Society of America, Special Paper, 388, pp. 449–462.
Ernst, R.E., Buchan, K.L., 2001. Large mafic magmatic events through time and links to mantle plume heads. In: Ernst, R.E., Buchan, K.L. (Eds.), Mantle Plumes: Their Identification through Time: Geological Society of America, Special Paper, 352, pp. 483–575.
Ernst, R.E., Buchan, K.L., Palmer, H.C., 1995. Giant dyke swarms. Characteristics, distribution and geotectonic applications. In: Baer, G., Heimann, A. (Eds.), Physics and Chemistry of Dykes. Balkema, Rotterdam, pp. 3–21.
Escrig, S., Capmas, F., Dupré, B., Allégre, C.J., 2004. Osmium isotopic constraints on the nature of the DUPAL anomaly from Indian mid-ocean-ridge basalts. Nature 431, 59–63.
Féraud, G., Giannerini, G., Campredon, R., 1987. Dyke swarms as paleostress indicators in areas adjacent to continental collision zones: examples from the European and

Northwest Arabian Plates. In: Halls, H.C., Fahrig, W.F. (Eds.), Mafic Dyke Swarms: Geological Association of Canada Special Paper, 34, pp. 273–278.
Gao, S., Luo, T.C., Zhang, B.R., Zhang, H.F., Han, Y.W., Zhao, Z.D., Hu, Y.K., 1998. Chemical composition of the continental crust as revealed by studies in East China. Geochimica et Cosmochimica Acta 62, 1959–1975.
Gao, S., Rudnick, R., Yuan, H.L., Liu, X.M., Liu, Y.S., Xu, W.L., Ling, W.L., Ayers, J., Wang, X.C., Wang, Q.H., 2004. Recycling lower continental crust in the north China craton. Nature 432, 892–897.
Gao, S., Rudnick, R.L., Xu, W.L., Yuan, H.L., Liu, Y.S., Walker, R.J., Puchtel, I., Liu, X.M., Huang, H., Wang, X.R., Yang, J., 2008. Recycling deep cratonic lithosphere and generation of intraplate magmatism in the North China Craton. Earth and Planetary Science Letters 270, 41–53.
Gudmunsson, A., 1995. Infrastructure and mechanics of volcanic systems in Iceland. Journal of Volcanology and Geothermal Research 64, 1–22.
Guo, J.-H., Sun, M., Chen, F.-K., Zhai, M.-G., 2005. Sm–Nd and SHRIMP U–Pb zircon geochronology of high-pressure granulites in the Sanggan area, North China Craton: timing of Palaeoproterozoic continental collision. Journal of Asian Earth Sciences 24, 629–642.
Halls, H.C., 1987. Dyke swarms and continental rifting some concluding remarks. In: Halls, H.C., Fahrig, W.F. (Eds.), Mafic Dyke Swarms: Geological Association of Canada Special Paper, 34, pp. 5–24.
Halls, H.C., Zhang, B., 2003. Crustal uplift in the southern Superior Province, Canada, revealed by paleomagnetism. Tectonophysics 362, 123–136.
Halls, H.C., Li, J., Davis, D., Hou, G., Zhang, B., Qian, X., 2000. A precisely dated Proterozoic palaeomagnetic pole forms the NCC, and its relevance to palaeocontinental reconstruction. Geophysical Journal International 143, 185–203.
Hanski, E., Mertanen, S., Ramo, T., Vuollo, J. (Eds.), 2006. Dyke Swarms - Time Markers of Crustal Evolution. Taylor & Francis, London.
Herzberg, C., Asimow, P.D., Arndt, N., Niu, Y., Lesher, C.M., Fitton, J.G., Cheadle, M.J., Saunders, A.D., 2007. Temperatures in ambient mantle and plumes: Constraints from basalts, picrites, and komatiites. Geochemistry, Geophysics, Geosystems 8, Q02006. doi:10.1029/2006GC001390.
Hirajima, T., Ishiwatari, A., Cong, B., Zhang, R., Banno, S., Nozaka, T., 1990. Coesite from Mengzhong eclogite at Donghai county, northern Jiangsu province, China. Mineralogical Magazine 54, 579–583.
Hou, G.T., Mu, Z.G., 1994. K–Ar ages and their geological significance of late-Precambrian mafic dyke swarms in north China Craton. Journal of Geology and Mineral Resources of North China 9, 267–270 (in Chinese with English abstract).
Hou, G.T., Zhang, C., Qian, X.L., 1998. The formation mechanism and tectonic stress field of the Mesoproterozoic mafic dyke swarms in the North China Craton. Geological Review 44, 309–314 (in Chinese with English abstract).
Hou, G.T., Li, J.H., Qian, X.L., 2001. Geochemical characteristics and tectonic setting of Mesoproterozoic dyke swarms in northern Shanxi. Acta Petrologica Sinica 77, 352–353 (in Chinese with English abstract).
Hou, G.T., Qian, X.L., Li, J.H., 2002. The simulation of Mesoproterozoic tectonic stress field forming mafic dyke swarms in the Central North China Craton. Acta Scientiarum Naturalium Universitatis Pekinesis 38, 492–496 (in Chinese with English abstract).
Hou, G.T., Li, J.H., Qian, X.L., 2003. The flow structures and mechanics of late Precambrian mafic dyke swarms in the North China Craton. Acta Geologica Sinica 77, 210–216.
Hou, G.T., Liu, Y.L., Li, J.H., 2006. Evidence for 1.8 Ga extension of the Eastern Block of the North China Craton from SHRIMP U–Pb dating of mafic dyke swarms in Shandong Province. Journal of Asian Earth Sciences 27, 392–401.
Jahn, B.M., Wu, F.Y., Lo, C.H., Tsai, C.H., 1999. Crust mantle interaction induced by deep subduction of the continental crust: geochemical and Sr–Nd isotopic evidence from post-collisional mafic-ultramafic intrusions of the northern Dabie complex, central China. Chemical Geology 157, 119–146.
John, D.A.P., Zhang, J.S., Huang, B.C., Andrew, P.R., 2010. Palaeomagnetism of Precambrian dyke swarms in the North China Shield: the 1.8 Ga LIP event and crustal consolidation in late Palaeoproterozoic times. Journal of Asian Earth Sciences 41, 504–524.
Jull, M., Kelemen, P.B., 2001. On the conditions for lower crustal convective instability. Journal of Geophysical Research 106, 423–446.
Kato, T., Enami, A., Zhai, M., 1997. Ultrahigh-pressure marble and eclogite in the Su-Lu ultrahigh-pressure terrane, eastern China. Journal of Metamorphic Geology 15, 169–182.
Kay, R.W., Kay, S.M., 1991. Creation and destruction of lower continental crust. Geologische Rundschau 80, 259–278.
Kogiso, T., Hirschmann, M.M., Frost, D.J., 2003. High-pressure partial melting of garnet pyroxenite: possible mafic lithologies in the source of ocean island basalts. Earth and Planetary Science Letters 216, 603–617.
Kroöner, A., Wilde, S.A., Li, J.-H., Wang, K.-Y., 2005. Age and evolution of a late Archaean to Palaeoproterozoic upper to lower crustal section in the Wutaishan/Hengshan/Fuping terrain of north China. Journal of Asian Earth Sciences 24, 567–576.
Kusky, T.M., Li, J.-H., 2003. Palaeoproterozoic tectonic evolution of the North China craton. Journal of Asian Earth Sciences 22, 383–397.
Kusky, T.M., Windley, B.F., Zhai, M.-G., 2007. In: Zhai, M.-G., Windley, B.F., Kusky, T.M., Meng, Q.-R. (Eds.), Tectonic evolution of the North China block: from orogen to craton to orogen. : Mesozoic Sub-Continental Lithospheric Thinning under Eastern Asia, 208. Geological Society Special Publications, pp. 1–34.
Levander, A., Niu, F., Lee, C.T.A., Cheng, X., 2006. Imaging the continental lithosphere. Tectonophysics 416, 167–185.
Li, J.-H., Qian, X.-L., Huang, X.-N., Liu, S.-W., 2000. The tectonic framework of the basement of north China craton and its implication for the early Precambrian cratonization. Acta Geologica Sinica 16, 1–10.
Li, J.H., Hou, G.T., Huang, X.N., Zhang, Z.Q., Qian, X.L., 2001. Precambrian geology of the North China Block. Acta Petrologica Sinica 17, 177–186 (in Chinese with English abstract).
Li, J.-H., Kusky, T.M., Huang, X.-N., 2002. Neoarchean podiform chromitites and mantle tectonites in ophiolitic melange, North China Craton: a record of early oceanic mantle oceanic mantle processes. GSA Today 12, 4–11.
Li, X.H., Li, Z.X., Li, W.X., Liu, Y., Yuan, C., Wei, G.J., Qi, C.S., 2007. U–Pb zircon, geochemical and Sr–Nd–Hf isotopic constraints on age and origin of Jurassic I- and A-type granites from central Guangdong, SE China: a major igneous event in response to foundering of a subducted flat-slab? Lithos 96, 186–204.
Li, T.S., Zhai, M.G., Peng, P., Chen, L., Guo, J.H., 2010. Ca. 2.5 billion year old coeval ultramafic-mafic and syenitic dykes in Eastern Hebei: implications for cratonization of the North China Craton. Precambrian Research 180, 143–155.
Liu, S., Hu, R.Z., Zhao, J.H., Feng, C.X., 2004. K–Ar Geochronology of Mesozoic mafic dikes in Shandong Province, Eastern China: implications for crustal extension. Acta Geologica Sinica 78, 1207–1213.
Liu, S., Zou, H.B., Hu, R.Z., Zhao, J.H., Feng, C.X., 2006. Mesozoic mafic dikes from the Shandong Peninsula, North China Craton: petrogenesis and tectonic implications. Geochemical Journal 40, 181–195.
Liu, S., Hu, R.-Z., Gao, S., Feng, C.-X., Qi, L., Zhong, H., Xiao, T., Qi, Y.-Q., Wang, T., Coulson, I.M., 2008a. Zircon U–Pb geochronology and major, trace elemental and Sr–Nd–Pb isotopic geochemistry of mafic dykes in western Shandong Province, east China: constraints on their petrogenesis and geodynamic significance. Chemical Geology 255, 329–345.
Liu, S., Hu, R., Gao, S., Feng, C., Qi, Y., Wang, T., Feng, G., Coulson, I.M., 2008b. U–Pb zircon age, geochemical and Sr–Nd–Pb–Hf isotopic constraints on age and origin of alkaline intrusions and associated mafic dikes from Sulu orogenic belt, Eastern China. Lithos 106, 365–379.
Liu, S., Hu, R., Gao, S., Feng, C., Yu, B., Feng, G., Qi, Y., Wang, T., Coulson, I.M., 2009. Petrogenesis of Late Mesozoic mafic dykes in the Jiaodong Peninsula, eastern North China Craton and implications for the foundering of lower crust. Lithos 113, 621–639.
Ludwig, K.R., 2003. User's manual for Isoplot/Ex, Version 3.00: A Geochronological Toolkit for Microsoft Excel: Berkeley Geochronology Center Special Publication, 4, pp. 1–70.
Lustrino, M., 2005. How the delamination and detachment of lower crust can influence basaltic magmatism. Earth-Science Reviews 72, 21–38.
Park, J.K., Buchan, K.L., Harlan, S.S., 1995. A proposed giant radiating dyke swarm fragmented by the separation of Laurentia and Australia based on paleomagnetism of ca. 780 Ma mafic intrusions in western North America. Earth and Planetary Science Letters 132, 129–139.
Peng, P., 2010. Reconstruction and interpretation of giant mafic dyke swarms: a case study of 1.78 Ga magmatism in the North China craton. : Geological Society Special Publication, 338. Geological Society, London, pp. 163–178.
Peng, P., Zhai, M.G., Zhang, H.F., Zhao, T.P., Ni, Z.Y., 2004. Geochemistry and geological significance of the 1.8 Ga mafic dyke swarms in the North China Craton: an example from the juncture of Shanxi, Hebei and Inner Mongolia. Acta Petrologica Sinica 20, 439–456 (in Chinese with English abstract).
Peng, P., Zhai, M.-G., Zhang, H.-F., Guo, J.-H., 2005. Geochronological constraints on the Palaeoproterozoic evolution of the North China Craton: SHRIMP zircon ages of different types of mafic dikes. International Geology Review 47, 492–508.
Peng, P., Zhai, M.G., Guo, J.H., Kusky, T., Zhao, T.P., 2007. Nature of mantle source contributions and crystal differentiation in the petrogenesis of the 1.78 Ga mafic dykes in the central North China craton. Gondwana Research 12, 29–46.
Peng, P., Zhai, M.-G., Li, Z., Wu, F.-Y., Hou, Q.-L., 2008. Neoproterozoic (~820 Ma) mafic dyke swarms in the North China craton: implication for a conjoint to the Rodinia supercontinent? Abstracts, 13th Gondwana Conference, Dali, China, pp. 160–161.
Peng, P., Guo, J.H., Zhai, M.G., Bleeker, W., 2010. Paleoproterozoic gabbronoritic and granitic magmatism in the northern margin of the North China craton: evidence of crust–mantle interaction. Precambrian Research 183, 635–659.
Peng, P., Bleeker, W., Ernst, R.E., Söderlund, U., McNicoll, V., 2011a. U–Pb baddeleyite ages, distribution and geochemistry of 925 Ma mafic dykes and 900 Ma sills in the North China craton: evidence for a Neoproterozoic mantle plume. Lithos 127, 210–221.
Peng, P., Zhai, M.G., Li, Q.L., Wu, F.Y., Hou, Q.L., Li, Z., Li, T.S., Zhang, Y.B., 2011b. Neoproterozoic (900 Ma) Sariwon sills in North Korea: geochronology, geochemistry and implications for the evolution of the south-eastern margin of the North China Craton. Gondwana Research 20, 243–254.
Qi, L., Hu, J., Grégoire, D.C., 2000. Determination of trace elements in granites by inductively coupled plasma mass spectrometry. Talanta 51, 507–513.
Qian, X.L., Chen, Y.P., 1987. Late Precambrian mafic dyke swarms of the North China Craton. In: Halls, H.C., Fahrig, W.F. (Eds.), Mafic Dyke Swarms: Geological Association of Canada Special Paper, 34, pp. 385–392.
Rapp, R.P., Shimizu, N., Norman, M.D., Applegate, G.S., 1999. Reaction between slab-derived melts and peridotite in the mantle wedge: experimental constraints at 3.8–GPa. Chemical Geology 160, 335–356.
Rapp, R.P., Shimizu, N., Norman, M.D., 2003. Growth of early continental crust by partial melting of eclogite. Nature 425, 605–609.
Rudnick, R.L., Fountain, D.M., 1995. Nature and composition of the continental crust: a lower crustal perspective. Reviews of Geophysics 33, 267–309.
Rudnick, R.L., Gao, S., 2003. Composition of the continental crust. In: Rudnick, R.L., Holland, H.D., Turekian, K.K. (Eds.), The Crust. : Treatise on the Geochemistry, vol. 3. Elsevier-Pergamon, Oxford, pp. 1–64.
Sobolev, A.V., Hofmann, A.W., Sobolev, S.V., Nikogosian, I.K., 2005. An olivine-free mantle source of Hawaiian shield basalts. Nature 434, 590–597.
Sobolev, A.V., Hofmann, A.W., Kuzmin, D.V., Yaxley, G.M., Arndt, N.T., Chung, S.L., Danyushevsky, L.V., Elliott, T., Frey, F.A., Garcia, M.O., Gurenko, A.A., Kamenetsky, V.S., Kerr, A.C., Krivolutskaya, N.A., Matvienkov, V.V., Nikogosian, I.K., Rocholl, A., Sigurdsson, I.A., Sushchevskaya, N.M., Teklay, M., 2007. The amount of recycled crust in sources of mantle-derived melts. Science 316, 412–417.

Sun, S.S., McDonough, W.F., 1989. Chemical and isotopic systematics of oceanic basalts: implications for mantle composition and processes. In: Saunders, A.D., Norry, M.J. (Eds.), Magmatism in the Ocean Basins. Geological Society Special Publications, pp. 313–345.
Taylor, S.R., McLennan, S.M., 1985. The Continental Crust: Its Composition and Evolution. Blackwell, Oxford Press, p. 312.
Wilde, S.A., Zhao, G.-C., Sun, M., 2002. Development of the North China craton during the Late Archaean and its final amalgamation at 1.8 Ga: some speculation on its position within a global Palaeoproterozoic supercontinent. Gondwana Research 5, 85–94.
Yang, J., Godard, G., Kienast, J.R., Lu, Y., Sun, J., 1993. Ultra high pressure 60 kbar magnesite-bearing garnet peridotites from northeastern Jiangsu, China. Journal of Geology 101, 541–554.
Yaxley, G.M., 2000. Experimental study of the phase and melting relations of homogeneous basalt plus peridotite mixtures and implications for the petrogenesis of flood basalts. Contributions to Mineralalogy and Petrology 139, 326–338.
Yaxley, G.M., Green, D.H., 1998. Reactions between eclogite and peridotite: mantle refertilisation by subduction of oceanic crust. Schweizerische Mineralogische und Petrographische Mitteilungen 78, 243–255.
Yuan, H.L., Gao, S., Liu, X.M., Li, H.M., Gunther, D., Wu, F.Y., 2004. Accurate U–Pb age and trace element determinations of zircon by laser ablation-inductively coupled plasma mass spectrometry. Geostandards Newsletter 28, 353–370.
Zhai, M.-G., Liu, W.-J., 2003. Palaeoproterozoic tectonic history of the North China craton: a review. Precambrian Research 122, 183–199.
Zhai, M.-G., Peng, P., 2007. Palaeoproterozoic events in the North China Craton. Acta Petrologica Sinica 23, 2665–2682.
Zhai, M.-G., Bian, A.-G., Zhao, T.-P., 2000. Amalgamation of the supercontinent of the North China craton and its break up during late–middle Proterozoic. Science in China (Series D) 43, 219–232.
Zhang, R.Y., Liou, J.G., Cong, B., 1994. Petrogenesis of garnet-bearing ultramafic rocks and associated eclogites in the Sulu ultrahigh-P metamorphic terrane, eastern China. Journal of Metamorphic Geology 12, 169–186.
Zhang, R.Y., Hirajima, T., Banno, S., Cong, B., Liou, J.G., 1995. Petrology of ultrahigh-pressure metamorphic rocks in southern Sulu region, eastern China. Journal of Metamorphic Geology 13, 659–675.
Zhang, H.F., Sun, M., Zhou, X.H., Ying, J.F., 2005. Geochemical constraints on the origin of Mesozoic alkaline intrusive complexes from the North China Craton and tectonic implications. Lithos 81, 297–317.
Zhao, G.-C., Wilde, S.A., Cawood, P.A., Sun, M., 2001. Archaean blocks and their boundaries in the North China craton: lithological, geochemical, structural and P–T path constraints and tectonic evolution. Precambrian Research 107, 45–73.
Zhao, G.C., Wilde, S.A., Cawood, P.A., Sun, M., 2002. SHRIMP U–Pb zircon ages of the Fuping complex: implications for Late Archean to Paleoproterozoic accretion and assembly of the North China Craton. American Journal of Science 302, 191–226.
Zhao, G.-C., Sun, M., Wilde, S.A., Li, S.-Z., 2005. Late Archaean to Palaeoproterozoic evolution of the North China craton: key issues revisited. Precambrian Research 136, 177–202.
Zhong, H., Zhu, W.G., Chu, Z.Y., He, D.F., Song, X.Y., 2007. Shrimp U-Pb zircon geochronology, geochemistry, and Nd-Sr isotopic study of contrasting granites in the Emeishan large igneous province, SW China. Chemical Geology 236, 112–133.